Maximizing backward somersault rotation in parallel bars

Hiro Hirabayayashi, Daisuke Takeshita

Affiliation: Department of Life Sciences (Sports Sciences), Graduate School of Arts and Sciences, University of Tokyo.

Address: The University of Tokyo, Building No. 9, 3-8-1, Komaba, Meguro-ku, Tokyo, 153-8902, Japan

Phone number: +81-3-5454-6133

Fax number: +81-3-5454-4317

Email: shiganai.hiro@gmail.com

KEYWORDS: Gymnastics, parallel bars, optimization, somersault, induced acceleration analysis

Word count: 3690

(intro: 222, method: 1070, result: 430, discussion: 1798, conclusion: 170)

This is preprint.

Abstract

Backward somersault dismount at parallel bars in artistic gymnastics is considered a fundamental movement for other advanced skills, such as double backward tucked and piked somersaults. We aimed to identify strategies to maximize the number of rotations in the backward somersault dismount through computer–based optimization. We first determined the best stunt and observed hip flexion in the middle of the stunt, which is an unlikely movement for gymnasts. To study the effect of this hip flexion, we performed optimization under additional constraints to suppress this hip flexion. Analyzing the similarities and differences between these two conditions revealed the following essential features in backward somersault dismount: 1) To increase the number of rotations, increasing the angular momentum is more effective than increasing flight time. 2) Wrist and shoulder coordination observed in both optimization conditions increased the angular momentum. 3) The hip flexion observed only in the first optimization increased the angular momentum through coordination among the wrist, shoulder, and hip joints.

Introduction

Backward somersault dismount at parallel bars in artistic gymnastics is considered a fundamental movement for other advanced skills, such as double backward tucked and piked somersaults. (Fig. 1). A typical sequence of backward somersault dismount at parallel bars starts with a still handstand on the parallel bars, followed by shoulder extension and takeoff from the parallel bars. The gymnasts need to have extended airtime and high angular momentum around the center of mass (CoM) for high-valued dismount skills.

Previous studies have revealed the relationships between judged scores and kinematic and/or kinetic variables in single and double backward somersault dismounts (Prassas 1995, Prassas and Papadopoulos 2001, Gervais and Dunn 2003). However, strategies to improve the performance still remain elusive.

This study investigated strategies to maximize the number of rotations in backward somersault dismounts by using computer–based optimization. We first determined the best stunt by optimization and observed hip flexion in the middle of the stunt, which gymnasts do not typically perform. To study the effect of this hip flexion, we performed another optimization under additional constraints suppressing hip flexion in the middle of the stunt. Computer-based optimization is suitable for this purpose because, in the actual analysis of gymnasts, to know whether a stunt performed by a gymnast is optimal, to impose constraints on the movement of gymnasts, and to have gymnasts optimize their performance under the constraints are infeasible.

Method

Model Configuration

A two-dimensional model of the human and parallel bars was developed to maximize somersault rotation (Fig. 2). The human model consisted of three segments representing the trunk, arms, and legs. The segments were connected at the wrist, shoulder, and hip joints. The wrist was assumed to be fixed on the parallel bars because gymnasts grasp parallel bars tightly with their hands. Inertial parameters of the body were determined based on the body mass and the lengths of the body segments of a male gymnast

(Ae et al. 1992). A linear spring and damper was used to represent the parallel bars (Linge et al. 2006). Positive directions for the joint angles were assumed as ulnar flexion for the wrist, extension for the shoulder, and flexion for the hip. All the angles were defined as zero in the handstand position. The origin of the displacement of the parallel bars y_{PB} is realized when no force is applied including gravitational force.

Each joint had a torque actuator that incorporated its physiological properties such as torque–angle and torque–angular velocity relationships. The torque of each actuator was determined by the method of Millard et al. (2019) (Fig. 3). The torque at a given instant was the sum of the active and passive torques, and the active torque was determined by the active state, joint angle, and angular velocity:

$$\tau_{Pos} = \tau_{PE} + \lambda\ \tau^{M}_{Pos}\ t^{A}_{Pos} t^{V}_{Pos}\ (0 \leq \lambda \leq 1) \tag{1}$$

$$\tau_{Neg} = \tau_{PE} + |\lambda|\ \tau^{M}_{Neg}\ t^{A}_{Neg} t^{V}_{Neg}\ (-1 \leq \lambda < 0), \tag{2}$$

where τ_{PE} is the passive torque, λ is the active state varying between -1 and 1, $\tau^{M}_{Pos/Neg}$ is a constant, $t^{A}_{Pos/Neg}, t^{V}_{Pos/Neg}$ are the normalized torque–angle and torque–velocity curves modeled with a Gaussian function and hyperbola, respectively.

A movement was simulated from a still handstand with the input of time series of the active state for each joint (Fig. 4). An optimizing algorithm with genetic algorithms and simulated annealing was developed to search for the best performance.

As the performance of a simulated movement, the number of rotations

N_r was defined as follows:

$$N_r = \frac{L_{CoM}|_{takeoff}}{2\pi I_{stretched}} T_{air}, \tag{3}$$

where $L_{CoM}|_{takeoff}$ is the angular momentum around the CoM at takeoff, $I_{stretched}$ is the moment of inertia of the stretched posture, and T_{air} is the airtime. The takeoff occurred when the displacement of the parallel bars y_{PB} was equal to zero and $\theta_{Body} > 180°$, where $\theta_{Body} := \theta_W + \theta_S$. T_{air} is defined as the time when the CoM reached the height of the CoM in a standing position on the ground which is 1.8 m below the parallel bars. The stretched posture is also defined as the standing position ($\theta_S = 180°$ and $\theta_H = 0°$).

N_r was suitable as the performance for the following two reasons: (1) larger N_r enables gymnasts to perform more difficult backward dismounts; and (2) when they perform tucked or piked dismounts, gymnasts can prepare for a suitable landing with larger N_r by stretching their bodies before landing, which requires extra rotations.

There were two condition for successful movement: (1) $|\theta_W| < 45°$ all the time, which otherwise was considered out of balance; and (2) $y_{PB} < 0$ all the time, because otherwise the parallel bars vibrated quickly and became unrealistic. The integration of Newton's equations of motion was terminated when the simulated movement broke either of the two conditions.

There were two optimizing conditions: (1) unconstrained condition using the aforedescribed method; and (2) hip–flexion suppressed condition, which yields an additional condition. The additional condition was $\theta_H < 0$ all the time while $\theta_{Body} < 180°$. The hip–flexion suppressed condition was used to study the effect of hip flexion in the middle of movement observed in the unconstrained condition, which actual gymnasts do not usually perform. In the figure legends, we denote the unconstrained condition as “Uncon” and the hip–flexion suppressed condition as “HFS.”

Contribution of joint torques to physical quantities

The contribution of joint torques to L_{CoM} and other quantities was analyzed as previously accomplished (Liu et al. 2006, Zajac et al. 2002, Hirashima 2011, Koike et al. 2019).

Generalized acceleration, including translational and angular acceleration, can be expressed using a linear combination of generalized forces, such as force and torque. For example, the angular acceleration of the wrist joint (α_W) can be expressed as

$$\alpha_W = A_{\alpha_W}^{\tau_W}\tau_W + A_{\alpha_W}^{\tau_S}\tau_S + A_{\alpha_W}^{\tau_H}\tau_H + A_{\alpha_W}^{F_{PB}}F_{PB} + C_{\alpha_W} \tag{4}$$

$$(= \alpha_W^{\tau_W} + \alpha_W^{\tau_S} + \alpha_W^{\tau_H} + \alpha_W^{F_{PB}} + C_{\alpha_W}), \tag{5}$$

where $A_{\alpha_W}^{\tau_W}, A_{\alpha_W}^{\tau_S}, A_{\alpha_W}^{\tau_H}, A_{\alpha_W}^{F_{PB}}$, and C_{α_W} are coefficients that do not involve generalized forces (τ_W, τ_S, τ_H, or F_{PB}). $\alpha_W^{\tau_W} (= A_{\alpha_W}^{\tau_W}\tau_W)$ is defined as the contribution of τ_W to α_W, and $\alpha_W^{\tau_S}, \alpha_W^{\tau_H}$, and $\alpha_W^{F_{PB}}$ are defined similarly. C_{α_W} contains the effects independent of joint torques and F_{PB} such as those of gravitational force and inertia. The angular acceleration of the shoulder and hip joints (α_S and α_H) and the acceleration of the parallel bars (a_{PB}) can be expressed similarly.

For the x coordinate of the CoM (x_{CoM}), the equation of motion is

$$Ma_{x_{CoM}} = F_x, \tag{6}$$

where $a_{x_{CoM}}$ is the horizontal acceleration of the CoM, and F_x is the horizontal force acting on the upper limb from the parallel bars (Fig. 5a). Since $x_{CoM} = x_{CoM}(\theta_W, \theta_S, \theta_H, y_{PB})$,

$$a_{x_{CoM}} = c_W\alpha_W + c_S\alpha_S + c_H\alpha_H + c_{PB}a_{PB} + d, \tag{7}$$

where c_W, c_S, c_H, c_{PB}, and d are coefficients that do not involve generalized accelerations. Therefore, from Equations 4–7

$$F_x = A_{F_x}^{\tau_W}\tau_W + A_{F_x}^{\tau_S}\tau_S + A_{F_x}^{\tau_H}\tau_H + A_{F_x}^{F_{PB}}F_{PB} + C_{F_x} \tag{8}$$

$$(= F_x^{\tau_W} + F_x^{\tau_S} + F_x^{\tau_H} + F_x^{F_{PB}} + C_{F_x}), \tag{9}$$

where $A_{F_x}^{\tau_W}, A_{F_x}^{\tau_S}, A_{F_x}^{\tau_H}, A_{F_x}^{F_{PB}}$, and C_{F_x} are coefficients that do not involve generalized forces. $F_x^{\tau_W}(= A_{F_x}^{\tau_W}\tau_W)$ is defined as the contribution of τ_W to F_x, and $F_x^{\tau_S}, F_x^{\tau_H}$, and $F_x^{F_{PB}}$ are defined similarly. C_{F_x} contains the effects independent of joint torques and F_{PB} such as those of gravitational force and inertia. From the equation of motion for the y coordinate of the CoM (y_{CoM}), the vertical force F_y acting on the upper limb from the parallel bars can be calculated in the same manner:

$$F_y = A_{F_y}^{\tau_W}\tau_W + A_{F_y}^{\tau_S}\tau_S + A_{F_y}^{\tau_H}\tau_H + A_{F_y}^{F_{PB}}F_{PB} + C_{F_y} \tag{10}$$

$$(= F_y^{\tau_W} + F_y^{\tau_S} + F_y^{\tau_H} + F_y^{F_{PB}} + C_{F_y}), \tag{11}$$

where $A_{F_y}^{\tau_W}, A_{F_y}^{\tau_S}, A_{F_y}^{\tau_H}, A_{F_y}^{F_{PB}}$, and C_{F_y} are coefficients that do not involve generalized forces. $F_y^{\tau_W}(= A_{F_y}^{\tau_W}\tau_W)$ is defined as the contribution of τ_W to F_y, and $F_y^{\tau_S}, F_y^{\tau_H}$, and $F_y^{F_{PB}}$ are defined similarly. C_{F_y} contains the effects independent of joint torques and F_{PB} such as those of gravitational force and inertia.

L_{CoM} satisfies the following equation:

$$\begin{aligned}\frac{dL_{CoM}}{dt} &= (\vec{p_W} - \vec{p_G}) \times \vec{F} + \tau_W \\ &= (y_{CoM} - y_{PB})F_x - x_{CoM}F_y + \tau_W \end{aligned} \tag{12}$$

where $\vec{p_G}$ and $\vec{p_W}$ are the position vectors of the CoM and wrist joint, and $\vec{F}$ is the external force vector at the wrist joint (Fig. 5b). Therefore, from Equation 8–12,

$$\frac{dL_{CoM}}{dt} = A^{\tau_W}_{dL_{CoM}}\tau_W + A^{\tau_S}_{dL_{CoM}}\tau_S + A^{\tau_H}_{dL_{CoM}}\tau_H + A^{F_{PB}}_{dL_{CoM}}F_{PB} + C_{dL_{CoM}}, \tag{13}$$

where $A^{\tau_W}_{dL_{CoM}}, A^{\tau_S}_{dL_{CoM}}, A^{\tau_H}_{dL_{CoM}}, A^{F_{PB}}_{dL_{CoM}}$, and $C_{dL_{CoM}}$ are coefficients that do not involve τ_W, τ_S, τ_H, or F_{PB}. $A^{\tau_W}_{dL_{CoM}}\tau_W$ is defined as the contribution of τ_W to the torque around the CoM, and $A^{\tau_S}_{dL_{CoM}}\tau_S, A^{\tau_H}_{dL_{CoM}}\tau_H$, and $F_y^{F_{PB}}$ are defined similarly. $C_{dL_{CoM}}$ contains the effects independent of joint torques and F_{PB} such as those of gravitational force and inertia. Because $A^{F_{PB}}_{dL_{CoM}}F_{PB}$ and $C_{dL_{CoM}}$ are independent of the joint torques, the sum of the two, $A^{F_{PB}}_{dL_{CoM}}F_{PB} + C_{dL_{CoM}}$, is referred to as the torque–independent term.

Furthermore, by integrating Equation 13, the contribution of the terms to L_{CoM} at t_2 with respect to t_1 can be calculated as

$$\begin{aligned}\int_{t_1}^{t_2} \frac{dL_{CoM}}{dt}dt = \int_{t_1}^{t_2} A^{\tau_W}_{dL_{CoM}}\tau_W dt + \int_{t_1}^{t_2} A^{\tau_S}_{dL_{CoM}}\tau_S dt + \int_{t_1}^{t_2} A^{\tau_H}_{dL_{CoM}}\tau_H dt \\ + \int_{t_1}^{t_2} \left(A^{F_{PB}}_{dL_{CoM}}F_{PB} + C_{dL_{CoM}}\right) dt.\end{aligned} \tag{14}$$

For instance, $\int_{t_1}^{t_2} A^{\tau_W}_{dL_{CoM}}\tau_W dt$ is considered the contribution of τ_W to L_{CoM}.

Let the time of takeoff be 0 and the time when L_{CoM} has the same value in the two optimizing conditions be $t_0(< 0)$. The difference in L_{CoM} between the two conditions at takeoff can then be expressed as

$$\Delta\left(L_{CoM}|_{t_0}^{0}\right) = \Delta\left(\int_{t_0}^{0} A_{dL_{CoM}}^{\tau_W}\tau_W dt\right) + \Delta\left(\int_{t_0}^{0} A_{dL_{CoM}}^{\tau_S}\tau_S dt\right) + \Delta\left(\int_{t_0}^{0} A_{dL_{CoM}}^{\tau_H}\tau_H dt\right) + \Delta\left(\int_{t_0}^{0} (A_{dL_{CoM}}^{F_{PB}}F_{PB} + C_{dL_{CoM}})dt\right), \tag{15}$$

where

$$\Delta\left(L_{CoM}|_{t_0}^{0}\right) = \left(L_{CoM}|_{t_0}^{0}\right)|_{Unconstrained} - \left(L_{CoM}|_{t_0}^{0}\right)|_{Hip-Flexion\ Suppressed} \tag{16}$$

and

$$L_{CoM}|_{t_0}^{0} = \int_{t_0}^{0} \frac{dL_{CoM}}{dt}dt. \tag{17}$$

The difference in L_{CoM} generation at takeoff due to τ_W can be expressed as $\Delta\left(\int_{t_0}^{0} A_{dL_{CoM}}^{\tau_W}\tau_W dt\right)$, and that due to the torque–independent term can be expressed as $\Delta\left(\int_{t_0}^{0}(A_{dL_{CoM}}^{F_{PB}}F_{PB} + C_{dL_{CoM}})dt\right)$.

According to the analysis of Equation 15, we inferred that the factors of the time series of θ_W were different between the unconstrained condition and the hip–flexion suppressed condition. The factors were examined considering

$$\Delta\alpha_W = \Delta(A_{\alpha_W}^{\tau_W}\tau_W) + \Delta(A_{\alpha_W}^{\tau_S}\tau_S) + \Delta(A_{\alpha_W}^{\tau_H}\tau_H) + \Delta(A_{\alpha_W}^{F_{PB}}F_{PB} + C_{\alpha_W}), \tag{18}$$

where

$$\Delta\alpha_W = \alpha_W|_{Unconstrained} - \alpha_W|_{Hip-Flexion\ Suppressed}.$$

Furthermore, the difference in θ_W caused the difference in τ_S, and the difference in τ_S caused the difference in ω_S. The factors causing the difference in ω_S were examined based on

$$\Delta\alpha_S = \Delta(A_{\alpha_S}^{\tau_W}\tau_W) + \Delta(A_{\alpha_S}^{\tau_S}\tau_S) + \Delta(A_{\alpha_S}^{\tau_H}\tau_H) + \Delta(A_{\alpha_S}^{F_{PB}}F_{PB} + C_{\alpha_S}) \quad (19)$$

where

$$\Delta\alpha_S = \alpha_S|_{Unconstrained} - \alpha_S|_{Hip-Flexion\ Suppressed}.$$

Result

The performance of the optimized movements in both conditions was sufficiently significant to perform the triple backward piked somersault (Fig. 6). This indicates successful optimization, given that the most successful backward somersault dismount by the real gymnasts is the double backward piked somersault (Fig. 1d). Although the difference in the performances between the two conditions appears small, it is remarkable because improving the already excellent performance is challenging.

The performance in the unconstrained condition was better than that in the hip–flexion suppressed condition (Table 1). This was expected as all of the movements satisfying the hip–flexion suppressed condition also satisfy the unconstrained condition. Although T_{air} in the unconstrained condition was shorter than that in the hip–flexion suppressed condition, the number of rotations was larger in the unconstrained condition because of its larger rotational velocity.

The number of rotations was positively correlated with $L_{CoM}|_{takeoff}$ but negatively correlated with T_{air} (Fig. 7), suggesting that increasing the $L_{CoM}|_{takeoff}$ was more crucial for increasing the number of rotations than increasing T_{air}. How to increase L_{CoM} is addressed in the Discussion section.

In the following description, time intervals are denoted by $[s, t]$, where s and t are the time before the takeoff. For example, $[-0.4\,\mathrm{s}, -0.2\,\mathrm{s}]$ represents the time interval from 0.4 s to 0.2 s before the takeoff.

There was a significant difference in θ_H between the unconstrained and hip–flexion suppressed conditions (Fig. 8). θ_H was positive at $[-0.4\,\mathrm{s}, -0.2\,\mathrm{s}]$ in the unconstrained condition, which any gymnast is unlikely to perform. We refer to this feature as hip flexion. On the contrary, θ_W and θ_S were similar in both conditions.

Concerning the active states, the wrist and hip active states were not similar, while those of the shoulder after $-0.8\,\mathrm{s}$ matched well (Fig. 9). The wrist active state decreased earlier in the unconstrained condition, although θ_W was similar. In contrast, the hip active state increased earlier in the unconstrained condition and held at the maximum for a longer duration than in the hip–flexion suppressed condition; thus, the hip flexion occurs only in the unconstrained condition.

y_{PB} was also remarkably similar to each other in the two conditions (Fig. 10). They were close to zero at $[-0.6\,\mathrm{s}, -0.4\,\mathrm{s}]$ and decreased quickly.

The change in L_{CoM} was similar to each other; it increased right after $-0.8\,\mathrm{s}$ and decreased after $-0.1\,\mathrm{s}$ (Fig. 11). We refer to this decrease in L_{CoM} after $-0.1\,\mathrm{s}$ as the "brake effect." The dominant factors increasing L_{CoM} were τ_S and the torque–independent term (Fig. 12). τ_S increased

L_{CoM} after $-0.8\,\mathrm{s}$ in both conditions, and the torque–independent term decreased L_{CoM} after $-0.1\,\mathrm{s}$. Thus, the torque–independent term appears to have caused the brake effect.

Discussion

We investigated strategies to increase the number of rotations in the backward somersault dismount performed at parallel bars. Because we found that increasing L_{CoM} appeared to be a better strategy for increasing the number of rotations than increasing T_{air}, we present the following two strategies to increase L_{CoM}: (1) Wrist and shoulder coordination observed in both conditions weaken the brake effect by activating their torques in order (2) Hip flexion observed only in the unconstrained condition increases L_{CoM} via the action–reaction law.

Wrist and shoulder coordination as a common strategy

The wrist and shoulder active states demonstrated a similar pattern in both conditions: the wrist active state was maintained at around 1 before $-0.8\,\mathrm{s}$, whereas the shoulder active state was maintained at around 1 after $-0.8\,\mathrm{s}$ (Fig. 9). We propose that this common feature provides a strategy for improving performance by minimizing the brake effect.

We analyzed the brake effect by decomposing it based on Equation 12; only τ_W was always positive at $[-0.1\,\mathrm{s},\ 0\,\mathrm{s}]$, whereas the other two terms, $(y_{CoM} - y_{PB})F_x$ and $-x_{CoM}F_y$, were mostly negative (Fig. 13). Decreasing $y_{CoM} - y_{PB}$ or increasing F_x would reduce the brake effect (Fig. 14), while decreasing x_{CoM} or F_y would also reduce the brake effect (Fig. 15).

Therefore, weakening of the brake effect could be achieved via four approaches: (1) decreasing $y_{CoM} - y_{PB}$, (2) decreasing F_y, (3) increasing F_x, and (4) decreasing x_{CoM}. However, we argue that (1), (2), and (3) are not effective in weakening the brake effect for high performance, whereas (4) is effective.

In (1), $y_{CoM} - y_{PB}$ is the vertical distance between the CoM and the wrist joint, as y_{PB} is identical to the vertical location of the wrist joint. Therefore, $y_{CoM} - y_{PB}$ is determined by the posture and inertial parameters of the body. $y_{CoM} - y_{PB}$ is minimized when $\theta_W = 0\ ^\circ, \theta_S = 180\ ^\circ$, and $\theta_H = 0\ ^\circ$. This posture would correspond to an action of pushing the body upright with the arms placed against the parallel bars, and it was already realized at approximately -0.15 s, which denotes a time period before the occurrence of the brake effect. Thus, decreasing $y_{CoM} - y_{PB}$ further may not be possible.

As regards (2), decreasing F_y would also reduce T_{air}, which may decrease performance.

With regard to (3), increasing F_x is not effective either because increasing F_x would also decrease F_y, as discussed below. First, F_x is proportional to $-F_y$ in [-0.1 s, 0 s]. This holds because F_x and F_y in [-0.1 s, 0 s] are almost equal to $F_x^{F_{PB}}$ and $F_y^{F_{PB}}$, respectively (Fig. 16). Therefore,

$$\frac{F_x}{F_y} \approx \frac{A_{F_x}^{F_{PB}}}{A_{F_y}^{F_{PB}}} \tag{20}$$

$$\because F_x \approx F_x^{F_{PB}} = A_{F_x}^{F_{PB}} F_{PB},\ F_y \approx F_y^{F_{PB}} = A_{F_y}^{F_{PB}} F_{PB} \tag{21}$$

$$\therefore F_x \propto F_y \tag{22}$$

Furthermore, because $F_x/F_y < 0$ in [-0.15 s, 0 s], $A_{F_x}^{F_{PB}}/A_{F_y}^{F_{PB}} < 0$ in

$[-0.15\,\mathrm{s}, 0\,\mathrm{s}]$. This indicates that increasing F_x would also reduce F_y, which would in turn reduce T_{air}.

As regards (4), decreasing x_{CoM} is achievable by generating a negative F_x before the occurrence of the brake effect, and its cumulative effect in reducing x_{CoM} is more significant when a negative F_x is generated as early as possible. According to Fig. 17, τ_W generated a negative F_x before $-0.8\,\mathrm{s}$, and τ_S generated a positive F_x after $-0.8\,\mathrm{s}$, which was suitable considering the cumulative effect.

However, a negative F_x would also reduce L_{CoM}, as $y_{CoM} - y_{PB} > 0$ (Equation 12). This indicates that τ_W reduced the brake effect by reducing x_{CoM} while reducing L_{CoM} with a negative F_x, and τ_S generated L_{CoM} with a positive F_x. This coordination pattern of τ_W and τ_S was caused by a unique feature of τ_W discussed below.

The effect of generating a negative F_x via joint torques on L_{CoM} can be evaluated by

$$\frac{A^{\tau(\cdot)}_{dL_{CoM}}}{A^{\tau(\cdot)}_{F_x}} \left(= \frac{A^{\tau(\cdot)}_{dL_{CoM}} \tau(\cdot)}{A^{\tau(\cdot)}_{F_x} \tau(\cdot)} = \frac{dL^{\tau(\cdot)}_{CoM}}{F^{\tau(\cdot)}_x} \right). \tag{23}$$

Reduction in $dL^{\tau(\cdot)}_{CoM}$ due to a negative $F^{\tau(\cdot)}_x$ is smaller for smaller $A^{\tau(\cdot)}_{dL_{CoM}}/A^{\tau(\cdot)}_{F_x}$ because

$$dL^{\tau(\cdot)}_{CoM} = \frac{A^{\tau(\cdot)}_{dL_{CoM}}}{A^{\tau(\cdot)}_{F_x}} F^{\tau(\cdot)}_x. \tag{24}$$

According to Fig. 18, $A^{\tau_W}_{dL_{CoM}}/A^{\tau_W}_{F_x}$ is smaller than $A^{\tau_S}_{dL_{CoM}}/A^{\tau_S}_{F_x}$ (note that $A^{\tau_H}_{dL_{CoM}}/A^{\tau_H}_{F_x}$ is remarkably similar to $A^{\tau_S}_{dL_{CoM}}/A^{\tau_S}_{F_x}$, although it is not plotted herein). This indicates that generating a negative F_x with τ_W is the best strategy to reduce x_{CoM} with less L_{CoM} reduction.

This unique feature of τ_W is attributable to the fact that the wrist joint is fixed on the parallel bars while neither the shoulder nor the hip joint has such a constraint. To clarify the difference, the torque around the CoM generated by τ_S is given as (Equation 12, Fig. 5b):

$$
\begin{aligned}
(y_{CoM} - y_{PB})F_x^{\tau_S} - x_{CoM}F_y^{\tau_S} &= \left[(y_{CoM} - y_{PB})A_{F_x}^{\tau_S} - x_{CoM}A_{F_y}^{\tau_S}\right]\tau_S \\
&= A_{dL_{CoM}}^{\tau_S}\tau_S. \qquad (25)
\end{aligned}
$$

As $-x_{CoM}A_{F_y}^{\tau_S}$ is sufficiently small compared with $(y_{CoM} - y_{PB})A_{F_x}^{\tau_S}$ (Fig. 19), the following approximation holds:

$$
\frac{A_{dL_{CoM}}^{\tau_S}}{A_{F_x}^{\tau_S}} \approx y_{CoM} - y_{PB}. \qquad (26)
$$

The same holds for τ_H (data not shown). In contrast, because the wrist joint is fixed on the parallel bars, the torque around the CoM generated by τ_W is as follows:

$$
\begin{aligned}
&(y_{CoM} - y_{PB})F_x^{\tau_W} - x_{CoM}F_y^{\tau_W} + \tau_W \\
&\qquad = \left[(y_{CoM} - y_{PB})A_{F_x}^{\tau_W} - x_{CoM}A_{F_y}^{\tau_W} + 1\right]\tau_W \\
&\qquad = A_{dL_{CoM}}^{\tau_W}\tau_W. \qquad (27)
\end{aligned}
$$

As $-x_{CoM}A_{F_y}^{\tau_W}$ is extremely small (data not shown), the following approximation holds:

$$
\frac{A_{dL_{CoM}}^{\tau_W}}{A_{F_x}^{\tau_W}} \approx y_{CoM} - y_{PB} + \frac{1}{A_{F_x}^{\tau_W}} \qquad (28)
$$

Furthermore, because $A_{F_x}^{\tau_W}$ is negative (Fig. 20), the following inequality holds:

$$\frac{A^{\tau_W}_{dL_{CoM}}}{A^{\tau_W}_{F_x}} - \frac{A^{\tau_S}_{dL_{CoM}}}{A^{\tau_S}_{F_x}} \approx \frac{1}{A^{\tau_W}_{F_x}} < 0, \tag{29}$$

$$\therefore \frac{A^{\tau_W}_{dL_{CoM}}}{A^{\tau_W}_{F_x}} < \frac{A^{\tau_S}_{dL_{CoM}}}{A^{\tau_S}_{F_x}}. \tag{30}$$

Therefore, τ_W can generate a negative F_x with a lower L_{CoM} reduction than τ_S or τ_H. Owing to this feature, τ_W before -0.8 s can successfully reduce x_{CoM} to weaken the brake effect (Fig. 21).

Alternatively, $A^{\tau_S}_{dL_{CoM}}/A^{\tau_S}_{F_x}$ and $A^{\tau_H}_{dL_{CoM}}/A^{\tau_H}_{F_x}$ are larger than $A^{\tau_W}_{dL_{CoM}}/A^{\tau_W}_{F_x}$. This implies that τ_S and τ_H can generate a certain amount of L_{CoM} with a less positive F_x than τ_W. A reduction in the positive F_x would also reduce x_{CoM}, resulting in weakening of the brake effect. Furthermore, because $A^{\tau_H}_{dL_{CoM}}$ is extremely small compared with the other terms (Fig. 22), generating a torque around the CoM via τ_S would be more effective than that via τ_H after -0.8 s.

In summary, the coordination between the wrist and shoulder joint appears to be a strategy for generating L_{CoM} while reducing the brake effect. The wrist first generates a negative F_x, and the shoulder then generates a positive F_x to effectively reduce the value of x_{CoM} considering the cumulative effect. The wrist generates a negative F_x because it generates the least L_{CoM} reduction with a negative F_x, and the shoulder generates a positive F_x because it generates the largest L_{CoM} production with a positive F_x.

Effect of hip flexion

To study the effect of hip flexion on performance, we first identified the factors responsible for the difference in L_{CoM} between the two conditions. Subsequently, we traced the factors back to hip flexion to understand how hip flexion increased L_{CoM} in the unconstrained condition.

To identify the factors causing the difference in L_{CoM} between the two conditions, we considered $-0.738\,\mathrm{s}$ as t_0 in Equation 15 to determine the breakdown of the contribution of joint torques to L_{CoM} . This was because the instant at -0.738 s occurred right before L_{CoM} started to increase consistently in both conditions, and L_{CoM} had the same value at -0.738 s (Fig. 11).

Based on the analysis conducted using Equation 15, we conclude that the difference in L_{CoM} resulted from the difference in the τ_W contribution (Table 2), and the τ_W contribution to L_{CoM} differed in $[-0.738\,\mathrm{s}, -0.4\,\mathrm{s}]$ (Fig. 23). From the breakdown of $A^{\tau_W}_{dL_{CoM}}\tau_W$ (Fig. 24), we conclude that the difference in the τ_W contribution to L_{CoM} resulted from the difference in τ_W itself, rather than that in $A^{\tau_W}_{dL_{CoM}}$. Furthermore, the difference in τ_W primarily resulted from the difference in the wrist active state, which can be inferred from the observation that the shape of the active state was similar to that of τ_W, while the changes in θ_W and ω_W were highly similar in both conditions (Fig. 25). The negative wrist active state in the unconstrained condition resulted in a negative τ_W, which generated additional L_{CoM} because $A^{\tau_W}_{L_{CoM}}$ was negative. In contrast, the positive wrist active state in the hip–flexion suppressed condition resulted in a positive τ_W, thereby generating a low value of L_{CoM}.

To understand why the positive wrist active state occurred in the hip–flexion suppressed condition at the expense of decreasing L_{CoM}, we replaced the wrist active state of the hip–flexion suppressed condition, with the unconstrained condition. Thereafter, the simulated movement resulted in a failure; the wrist angle quickly became less than $-45°$, and the gymnast did not manage to take off from the parallel bars. (Fig. 26). This result suggests that, in the hip–flexion suppressed condition, a positive wrist active state is necessary for successful movement and that, in the unconstrained condition, the effect of a negative wrist active state resulting in a lower value of θ_W is compensated by other factors.

To comprehend what factors aided in maintaining θ_W larger than $-45°$ in the unconstrained condition, we analyzed the value of α_W that directly affected θ_W. The analysis based on Equation 18 revealed that the difference in τ_S contribution to α_W was the most significant among all the other terms, and it was positive in $[-0.8\,\mathrm{s}, -0.7\,\mathrm{s}]$, which rendered the value of α_W in the unconstrained condition larger (Fig. 27). This indicates that τ_S maintained the value of θ_W larger than $-45°$ in the unconstrained condition. The difference in the τ_S contribution to α_W resulted from the difference in τ_S itself (Fig. 28). τ_S affected α_W through the action–reaction law; when τ_S was applied to the trunk segment, $-\tau_S$ was applied to the arm segment. Furthermore, the difference in τ_S resulted from the difference in the shoulder active state because the shape of the active state was similar to that of τ_S in both conditions, while the difference in θ_S or ω_S between the two conditions was not sufficiently large to affect the maximal torque in the two conditions (Fig. 29).

A smaller τ_S generating a larger α_W in the unconstrained condition made the realization of a negative τ_W possible, resulting in a higher contribution of τ_W to L_{CoM}. Simultaneously, a smaller value of τ_S reduced the τ_S contribution to L_{CoM} because $A^{\tau_S}_{dL_{CoM}}$ was positive (Fig. 30). However, the total

τ_S contribution to L_{CoM} evaluated at takeoff was larger in the unconstrained condition (Fig. 23, 31). Until $-0.5\,\mathrm{s}$, τ_S in the hip–flexion suppressed condition contributed more to L_{CoM}. In contrast, in $[-0.5\,\mathrm{s},\ -0.3\,\mathrm{s}]$, the unconstrained condition gained approximately 4 $\mathrm{N \cdot m \cdot s}$ more L_{CoM} by τ_S than the hip–flexion suppressed condition, thereby ending up with larger L_{CoM} at takeoff. This was because τ_S in the unconstrained condition was larger in $[-0.5\,\mathrm{s},\ -0.3\,\mathrm{s}]$, and $A^{\tau_S}_{dL_{CoM}}$ was almost the same in both conditions. Given that the shoulder active state is maximal in both conditions (Fig. 32), a larger τ_S in the unconstrained condition was primarily caused by a smaller ω_S in the unconstrained condition through torque–angular velocity relationships (Fig. 3d).

To understand why ω_S was smaller in the unconstrained condition than in the hip–flexion suppressed condition, we quantified the contribution of each joint torque to α_S based on Equation 19. The largest difference between the two conditions was that of τ_H, and it was smaller in the unconstrained condition, leading to a lower value of ω_S in the unconstrained condition. (Fig. 33). The difference in $A^{\tau_H}_{\alpha_S}\tau_H$ primarily resulted from the difference in τ_H (Fig. 34). Note that τ_H affected α_S through the action–reaction law; when τ_H was applied to the leg segment, $-\tau_H$ was applied to the body segment, thereby decreasing α_S.

Furthermore, the difference in τ_H resulted from the hip active state because only the shape of the active state was sufficiently affected to render a larger value of τ_H in the unconstrained condition (Fig. 35); the difference in θ_H did not result in a larger value for τ_H in the unconstrained condition because the difference in the maximal τ_H resulting from the θ_H difference was approximately 15 $\mathrm{N \cdot m}$, and this was not enough to make τ_H larger in the unconstrained condition. For ω_H, a larger ω_H in the unconstrained condition made the maximum τ_H in the unconstrained condition smaller, regardless of whether the hip active state was positive or negative (Fig. 3f).

In summary, hip flexion increased L_{CoM} through coordination between the wrist, shoulder, and hip joints. The underlying mechanism can be outlined as follows:

1. The unconstrained condition gained a larger value of L_{CoM} than the hip–flexion suppressed condition by lowering τ_W.

2. Lowering τ_W required the unconstrained condition to lower τ_S to maintain $\theta_W > -45°$ because a large positive τ_S would have generated a negative value of α_W and made θ_W smaller.

3. However, a lower value of τ_S in the unconstrained condition also reduced the τ_S contribution to L_{CoM}. To attain the same amount of contribution to L_{CoM}, τ_S had to be increased at some point between lowering τ_W and takeoff.

4. The unconstrained condition successfully gained τ_S owing to its larger τ_H that lowered ω_S in the unconstrained condition through action–reaction law.

5. The larger τ_H in the unconstrained condition caused visible hip flexion.

CONCLUSION

The aim of this study was to identify strategies to maximize the number of rotations in the backward somersault dismount at parallel bars in artistic gymnastics. Through computer-based optimization, we found that increasing the angular momentum is more effective than increasing flight time to increase the number of rotations. We further identified that strategies such as hip flexion in the middle of a stunt and the sequential production of wrist ulnar flexion torque, followed by shoulder extension torque, contribute to gaining the angular momentum.

However, in reality, no gymnasts are likely to perform this hip flexion. Thus, our future task involves identifying the reason for the same. One possibility is that this hip flexion requires gymnasts to precisely maintain their balance—any movements with hip flexion in the middle of a stunt may present a high risk of their shoulder falling under the parallel bars. A method to evaluate the difficulty faced by gymnasts in maintaining balance during a stunt needs to be developed to study such aspects.

ACKNOWLEDGMENTS

This work was partially supported by JSPS KAKENHI Grant Number JP20K11330. We also would like to thank the members of the Sports Biomechanics Lab at the University of Tokyo for helpful discussions.

References

Ae, M., Tang, H., Yokoi, T., 1992. Estimation of inertia properties of the body segments in japanese athletes. Biomechanisms 11, 23–33.

Gervais, P., Dunn, J., 2003. Gymnastics: The double back salto dismount from the parallel bars. Sports biomechanics 2(1), 85–101.

Hirashima, M., 2011. Induced acceleration analysis of three-dimensional multi-joint movements and its application to sports movements. In: Klika, V., Theoretical Biomechanics, IntechOpen, Rijeka, chapter 14.

Koike, S., Ishikawa, T., Willmott, A. P., Bezodis, N. E., 2019. Direct and indirect effects of joint torque inputs during an induced speed analysis of a swinging motion. Journal of biomechanics 86, 8–16.

Linge, S., Hallingstad, O., Solberg, F., 2006. Modelling the parallel bars in men ' s artistic gymnastics. Human movement science 25(2), 221–237.

Liu, M. Q., Anderson, F. C., Pandy, M. G., Delp, S. L., 2006. Muscles that support the body also modulate forward progression during walking. Journal of biomechanics 39(14), 2623–2630.

Millard, M., Emonds, A. L., Harant, M., Mombaur, K., 2019. A reduced muscle model and planar musculoskeletal model fit for the simulation of whole-body movements. Journal of biomechanics 89, 11–20.

Prassas, S., Papadopoulos, C., 01 2001. Mechanics of forward support swing skills on the parallel bars. Journal of Human Movement Studies 40, 335–350.

Prassas, S. G., 1995. Technique analysis of the 1992 compulsory dismount from the parallel bars. In ISBS-Conference Proceedings Archive.

Zajac, F. E., Neptune, R. R., Kautz, S. A., 2002. Biomechanics and muscle coordination of human walking: Part i: Introduction to concepts, power transfer, dynamics and simulations. Gait & posture 16(3), 215–232.

Table 1: Best performances in the two conditions following Equation 3. Note that rotational velocity is equal to $\frac{L_{CoM}|_{takeoff}}{2\times\pi\times I_{stretched}}$.

condition	number of rotation	rotational velocity [s^{-1}]	airtime [s]
unconstrained	1.26	1.46	0.856
hip–flexion suppressed	1.22	1.40	0.871

Table 2: Values in Equation 15 where $t_0 = -0.738\,\mathrm{s}$. The positive value means that the unconstrained condition generates more L_{CoM} than the hip–flexion suppressed condition.

term	value
$\Delta\left(\int_{t_0}^{0} A_{dL_{CoM}}^{\tau_W}\tau_W\, dt\right)$	8.09
$\Delta\left(\int_{t_0}^{0} A_{dL_{CoM}}^{\tau_S}\tau_S dt\right)$	2.12
$\Delta\left(\int_{t_0}^{0} A_{dL_{CoM}}^{\tau_H}\tau_H dt\right)$	-0.662
$\Delta\left(\int_{t_0}^{0}(A_{dL_{CoM}}^{F_{PB}}F_{PB} + C_{dL_{CoM}})dt\right)$	-2.46

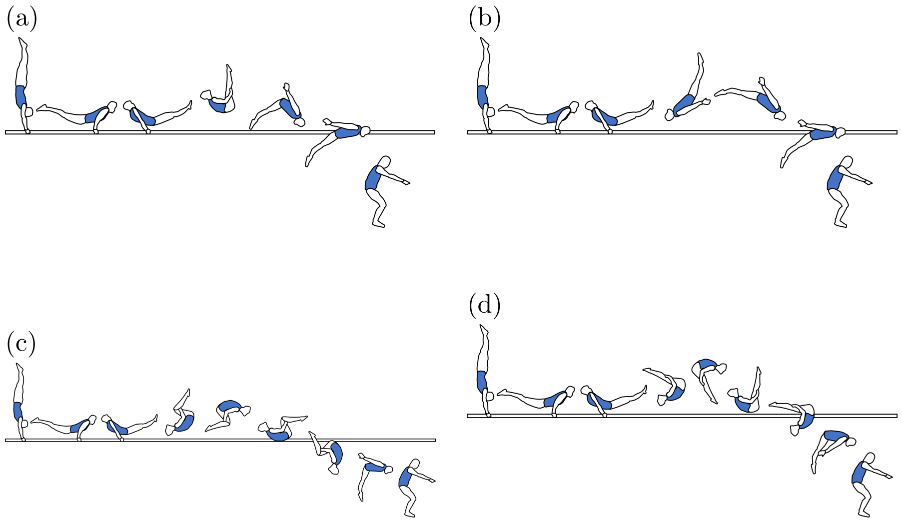

Figure 1: Examples of backward somersault dismounts sorted by their difficulty. (a) Single backward piked somersault (the easiest). (b) Single backward stretched somersault. (c) Double backward tucked somersault. (d) Double backward piked somersault (the most difficult). For any of the backward dismounts, the gymnasts begin with handstands and swing down their entire body until takeoff while supporting their body above the parallel bars. The moment of inertia decreases in the order of the stretched, piked, and tucked postures. The difficulty is valued by combining the moment of inertia and the number of rotations. Although the moment of inertia in the tucked posture is smaller than in the stretched posture, the difficulty corresponding to (c) is greater than that corresponding to (b) because the number of rotations is larger in (c). (d) is the most difficult dismount among the backward dismounts performed by real gymnasts.

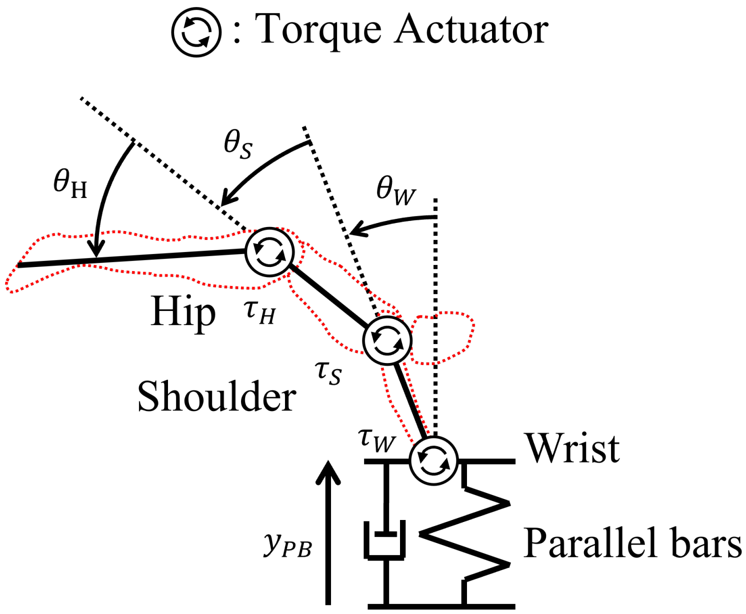

Figure 2: Simulated model. The model consists of a gymnast and parallel bars. The gymnast is modeled as three linked segments with the wrist, shoulder, and hip joints. Each joint has a torque actuator with its physiological characteristics. The parallel bars are modeled using a linear spring and damper. The angles of all the joints $(\theta_W, \theta_S, \theta_H)$ are defined, with zeros corresponding to the handstand posture. The positives are considered in ulnar flexion for the wrist, extension for the shoulder, and flexion for the hip.

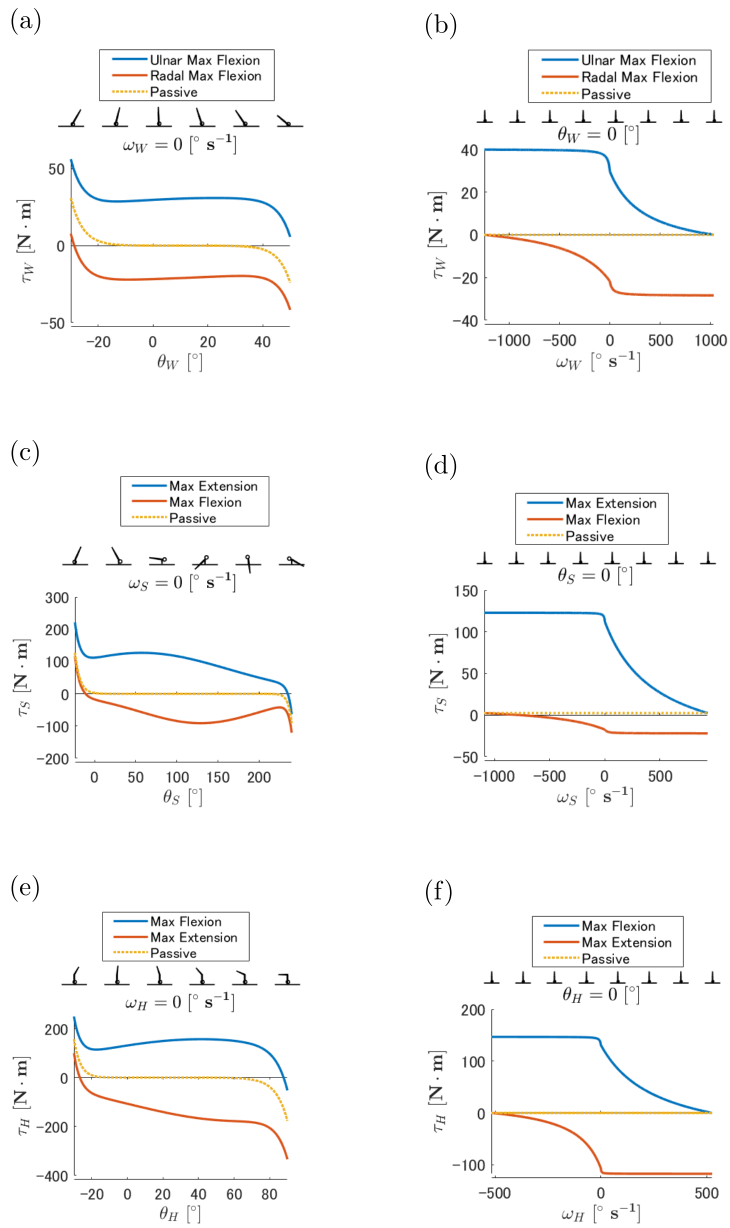

Figure 3: Physiological properties incorporated into the toque actuators. (3a), (3c), (3e) Torque–angle relationship for the wrist, shoulder, and hip, respectively. (3b), (3d), (3f) Torque–angular velocity relationship for the wrist, shoulder, and hip, respectively. The torque–angle relationships do not affect τ significantly when θ is far from the edge of the motion range. The torque–angular velocity relationships also do not affect τ significantly under eccentric ω. However, they change τ significantly under concentric ω

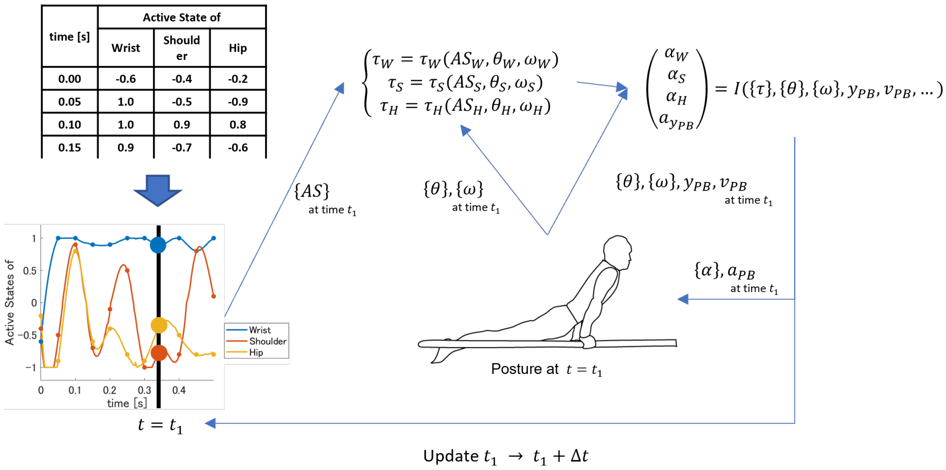

Figure 4: Simulation Flow. A time series of the active state for each joint with a 1/20 s resolution is used as input (upper left). Cubic spline interpolation is used to obtain a time series (lower left). To simulate the state at $t = t_1$, the joint torque (τ) for each joint is calculated considering the active states and the torque–angle–angular velocity relationships with θ and ω (top middle). The obtained joint torques are used for numerically integrating Newton's Equations, and the angles and angular velocities are obtained.

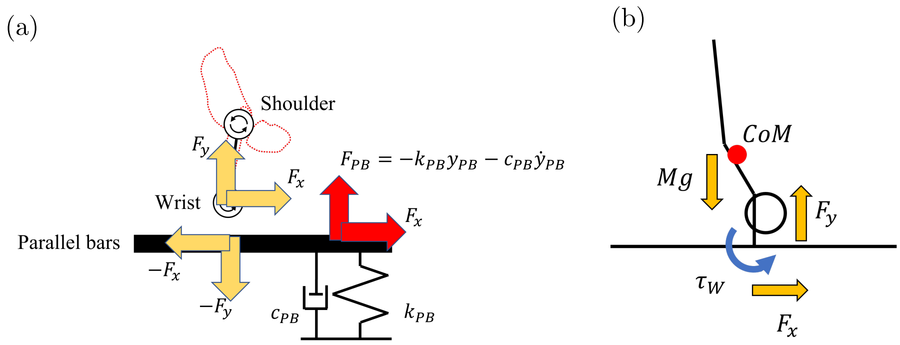

Figure 5: Illustration of external forces and torque acting on the gymnast. (a): Definition of F_{PB}, F_x, and F_y. Note that F_{PB} is a vertical force acting from the spring–damper element to the parallel bars, and F_x and F_y are the horizontal and vertical forces acting from the parallel bars to the wrist joint. F_y does not always match with F_{PB} because the parallel bars have mass and move vertically ($m_{PB}\ddot{y}_{PB} = F_{PB} - F_y$). However, the horizontal force between the spring-damper element and the parallel bars always matches with F_x because the parallel bars do not move horizontally. (b): The external forces and torque that affect L_{CoM} are displayed. The gravity acting on the gymnast does not affect L_{CoM} because the gravity applies to the CoM, creating no torque around the CoM. F_x and F_y affect L_{CoM} with a non-zero moment arm, and τ_W directly affects L_{CoM}.

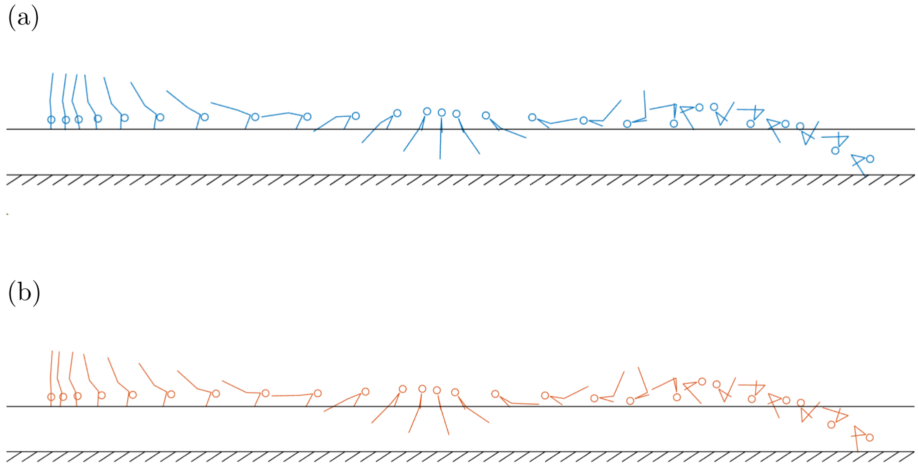

Figure 6: Simulated performance of the optimization results in the piked posture to compare the difficulty with Fig. 1d. (a) Best performance in the unconstrained condition in the piked posture. (b) Best performance in the hip–flexion suppressed condition in the piked posture. Both of the performances qualified triple backward piked somersault dismount. (a) was better than (b) because (a) had enough rotation to stretch the body to prepare for landing while (b) did not have enough rotation to stretch the body for landing.

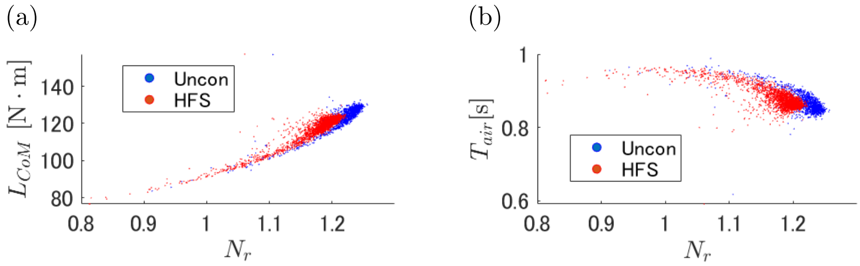

Figure 7: (a) N_r vs. $L_{CoM}|_{takeoff}$. (b) N_r vs. T_{air}. The results whose $N_r > 0.8$ found in the two optimizations were plotted.

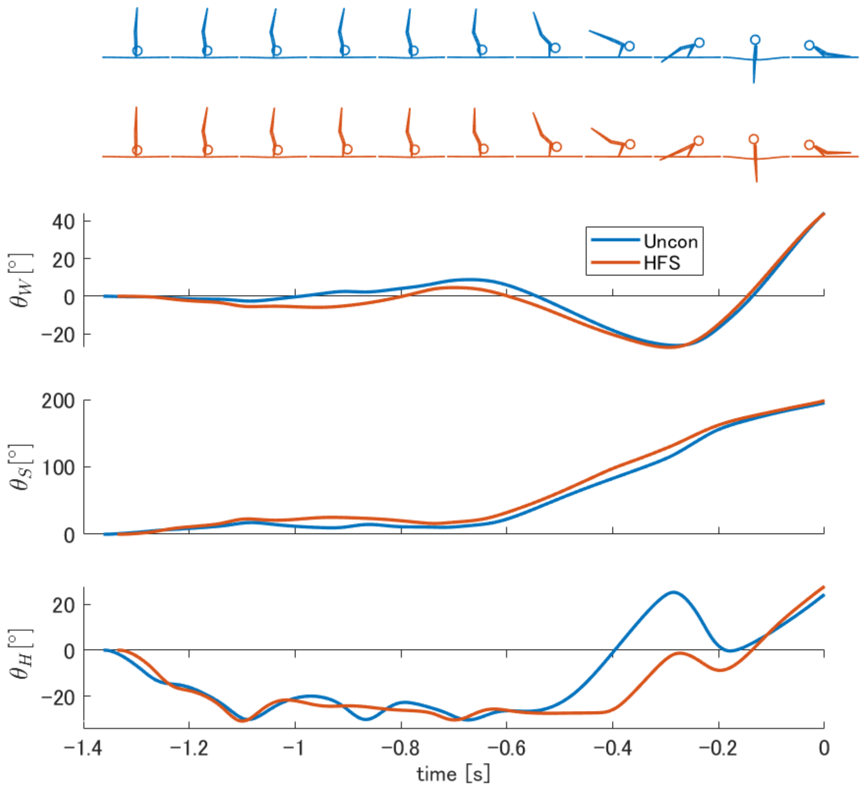

Figure 8: Joint angles of the wrist, shoulder, and hip in the unconstrained (blue) and the hip–flexion suppressed (red) conditions.

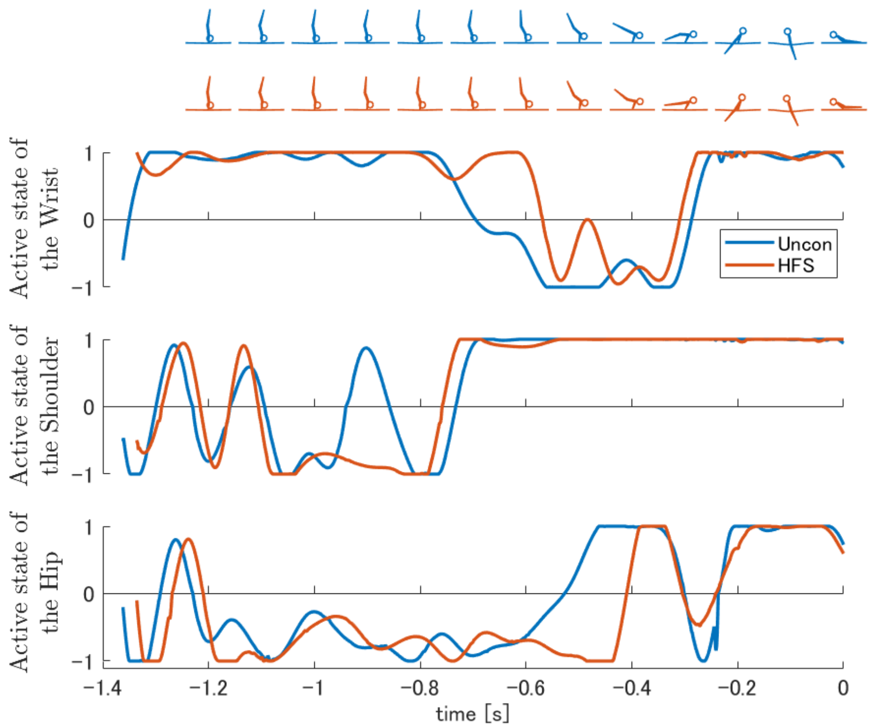

Figure 9: Active states of the wrist, shoulder, and hip in the unconstrained (blue) and the hip–flexion suppressed (red) conditions.

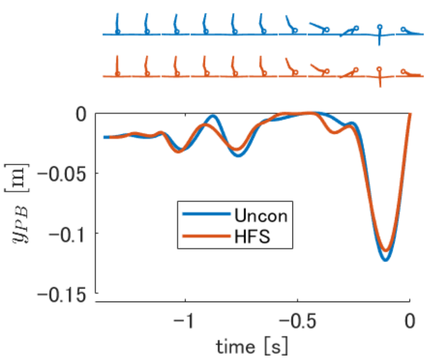

Figure 10: y_{PB} in the unconstrained (blue) and the hip–flexion suppressed (red) conditions. Note that y_{PB} is always maintained negative until takeoff because keeping $y_{PB} < 0$ is a common restriction in both conditions.

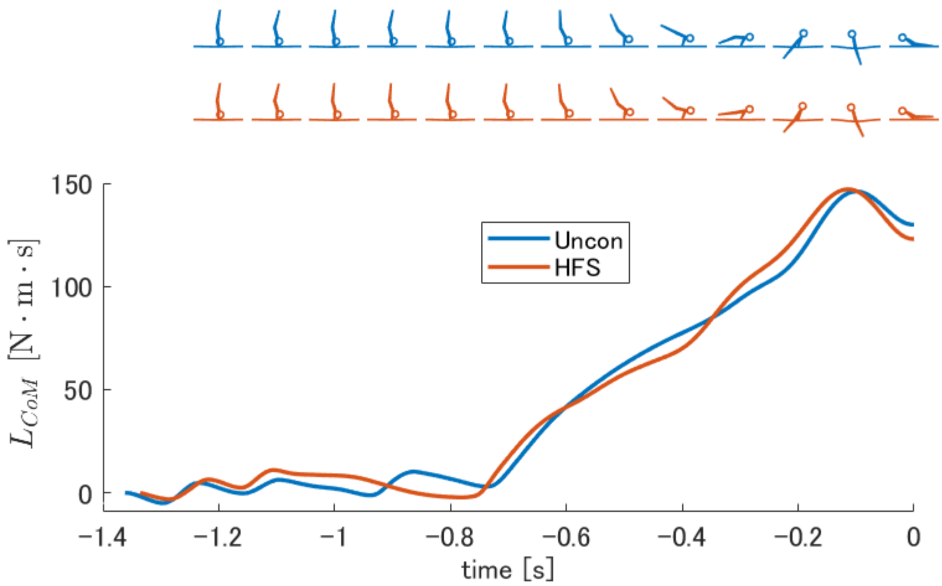

Figure 11: Angular momentum around the CoM (L_{CoM}) in the unconstrained (blue) and the hip–flexion suppressed (red) conditions.

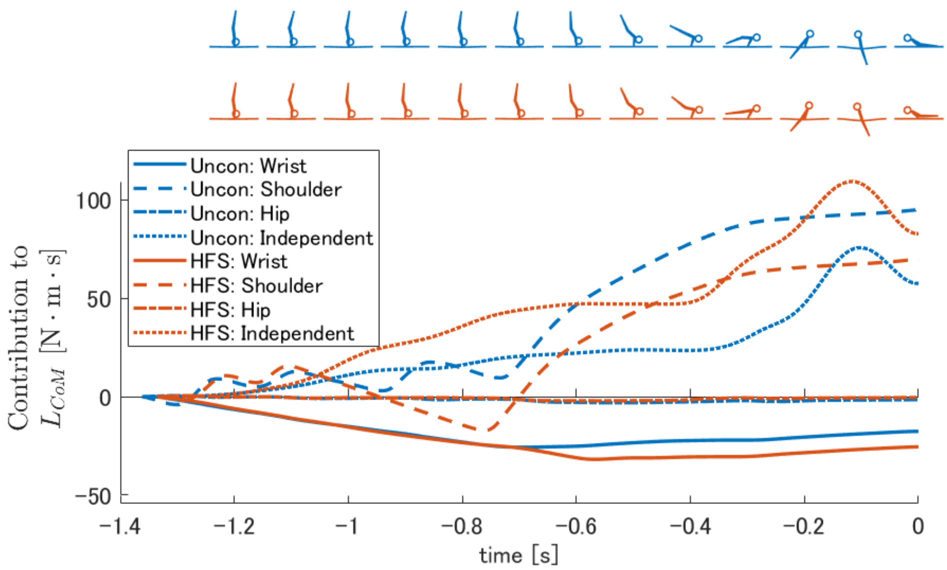

Figure 12: Contributions of the wrist, shoulder, hip joint torques, and the torque–independent term to L_{CoM} in Equation 14, with t_1 being the start of the motion.

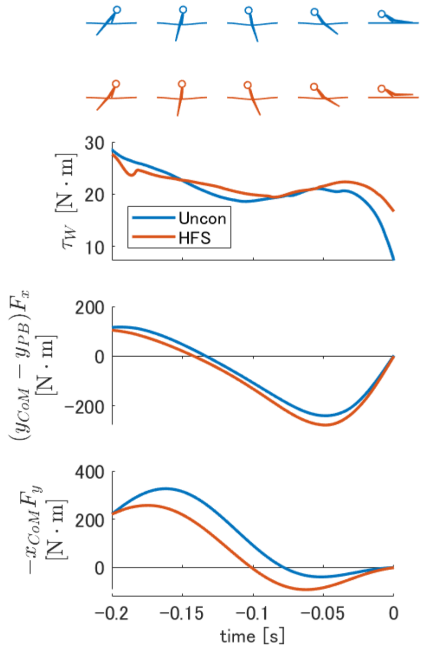

Figure 13: Decomposition of torque around the CoM based on Equation 12. From the top, τ_W, $(y_{CoM} - y_{PB})F_x$, and $-x_{CoM}F_y$ are presented. The positive value corresponds to increasing L_{CoM}.

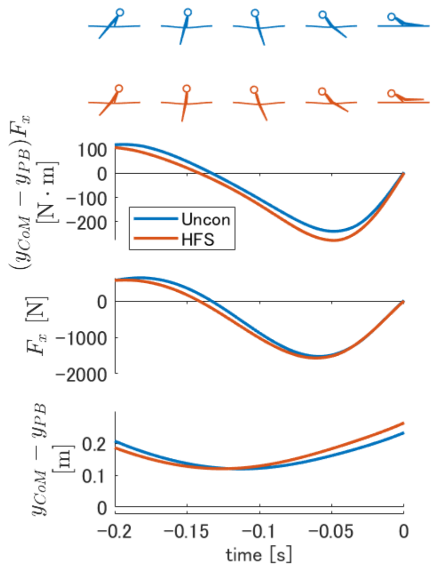

Figure 14: Breakdown of $(y_{CoM} - y_{PB})F_x$ into F_x and $y_{CoM} - y_{PB}$. From the top, $(y_{CoM} - y_{PB})F_x$, F_x, and $y_{CoM} - y_{PB}$ are presented.

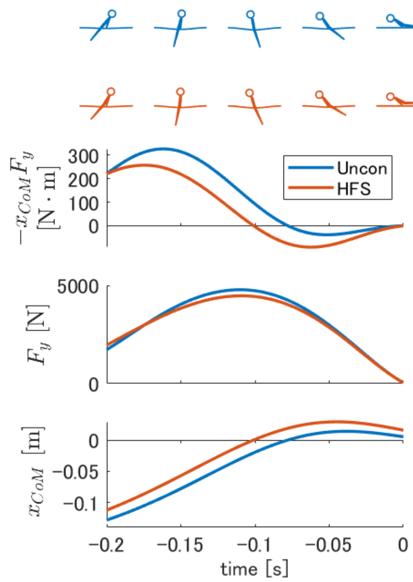

Figure 15: Breakdown of $-x_{CoM}F_y$ into F_y and x_{CoM}. From the top, $-x_{CoM}F_y$, F_y, and x_{CoM} are illustrated.

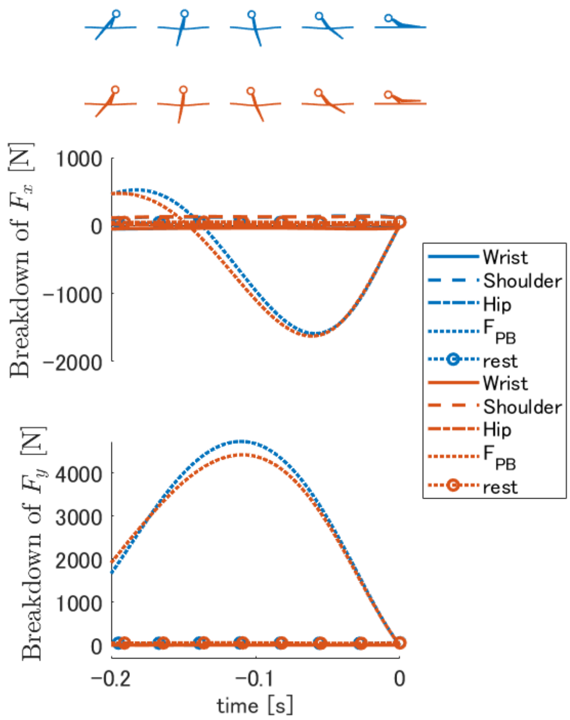

Figure 16: Breakdown of F_x and F_y into the contribution of the wrist, shoulder, hip joint torques, F_{PB}, and the remaining terms in $[-0.2\,\mathrm{s},\ 0\,\mathrm{s}]$. From the top, the breakdown of F_x and that of F_y are presented.

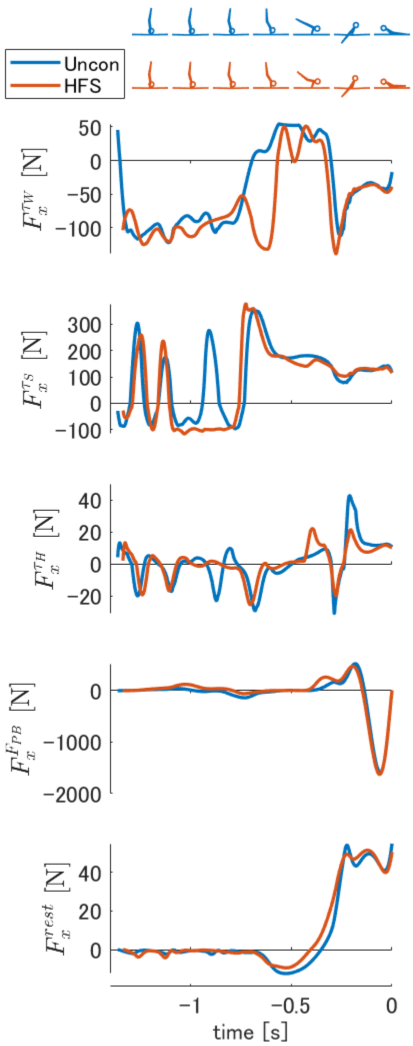

Figure 17: Breakdown of F_x into the contribution of the wrist, shoulder, and hip torques, as well as F_{PB}, and the remaining terms.

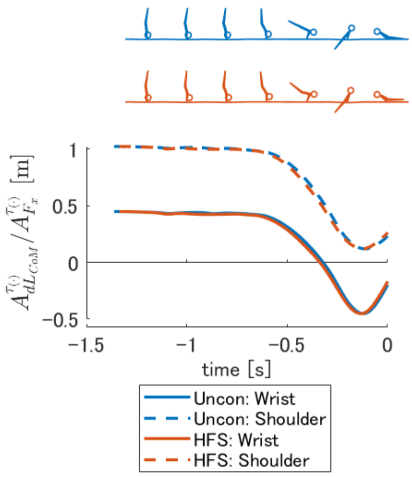

Figure 18: Ratio of the coefficients of contribution to the torque around the CoM ($= A^{\tau(\cdot)}_{dL_{CoM}}$) to F_x ($= A^{\tau(\cdot)}_{F_x}$). The larger the value, the lower the magnitude of F_x that needs to be generated to gain a certain amount of torque around the CoM.

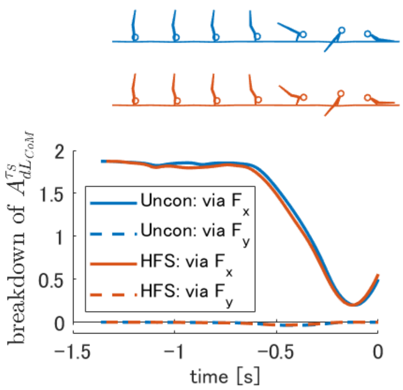

Figure 19: Breakdown of $A^{\tau_S}_{dL_{CoM}}$ into terms via F_x and F_y. Note that the terms obtained via F_x are equal to $(y_{CoM} - y_{PB})A^{\tau_S}_{F_x}$, and the terms obtained via F_y are equal to $-x_{CoM}A^{\tau_S}_{F_y}$.

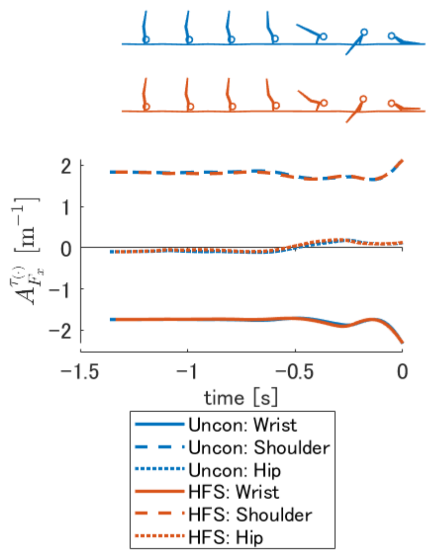

Figure 20: Coefficients of contribution of the wrist, shoulder, and hip torques to F_x .

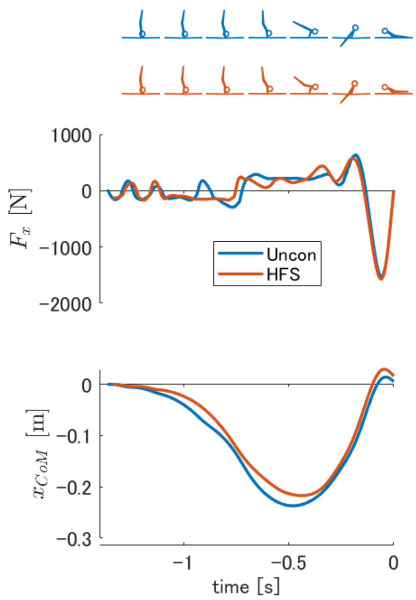

Figure 21: Horizontal force ($= F_x$) and horizontal position of the CoM ($= x_{CoM}$). From the top, F_x and x_{CoM} are presented. F_x tends to be negative at [start of motion, -0.8 s], and it tends to be positive at [-0.7 s, -0.2 s], which makes x_{CoM} downward convex.

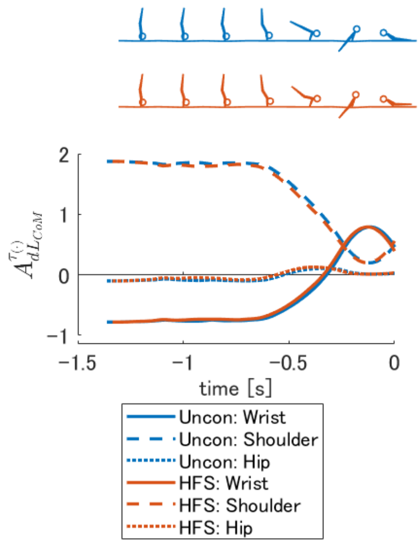

Figure 22: Coefficients of contribution of the wrist, shoulder, and hip to the torque around the CoM ($= dL_{CoM}$).

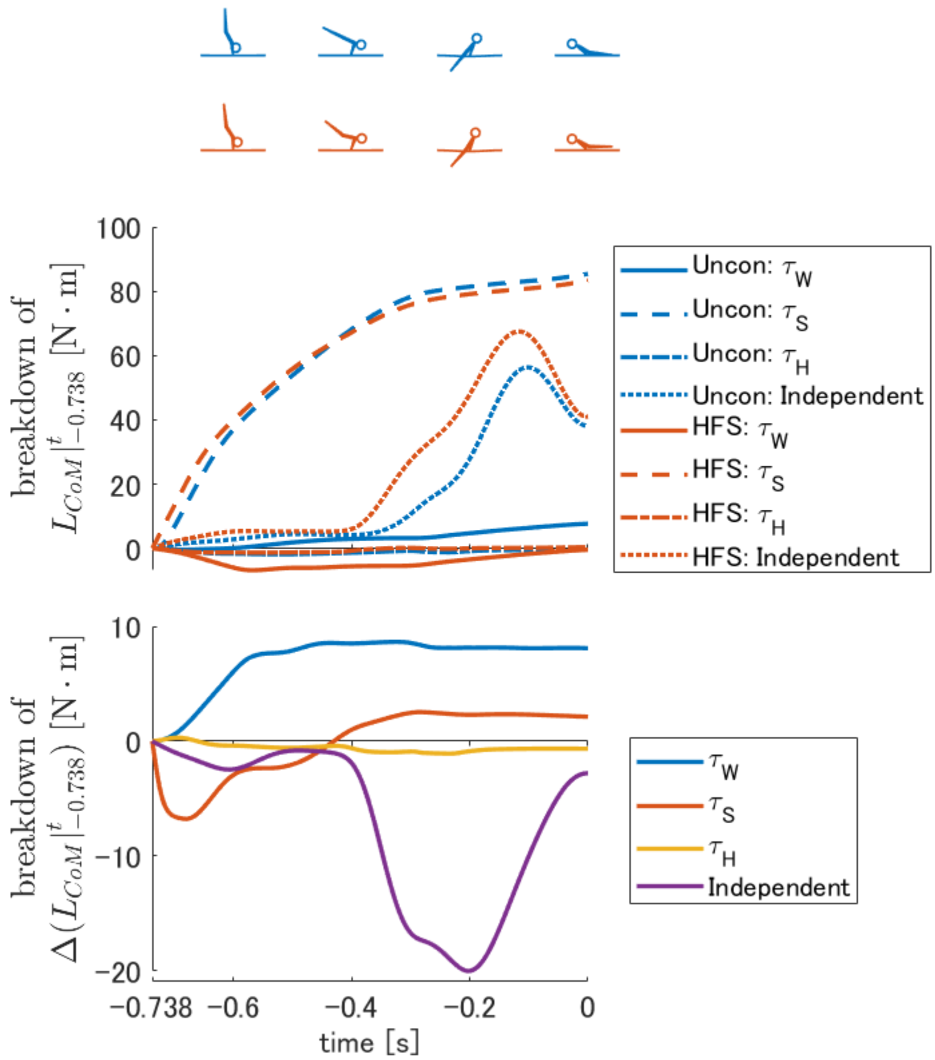

Figure 23: Top:breakdown of $L_{CoM}|^{t}_{-0.738\,\mathrm{s}}$ (Equation 14) into the terms of τ_W, τ_S, τ_H, and torque–independent term. Bottom: breakdown of $\Delta(L_{CoM}|^{t}_{-0.738\,\mathrm{s}})$ (Equation 15) into the terms of τ_W, τ_S, τ_H, and torque–independent term.

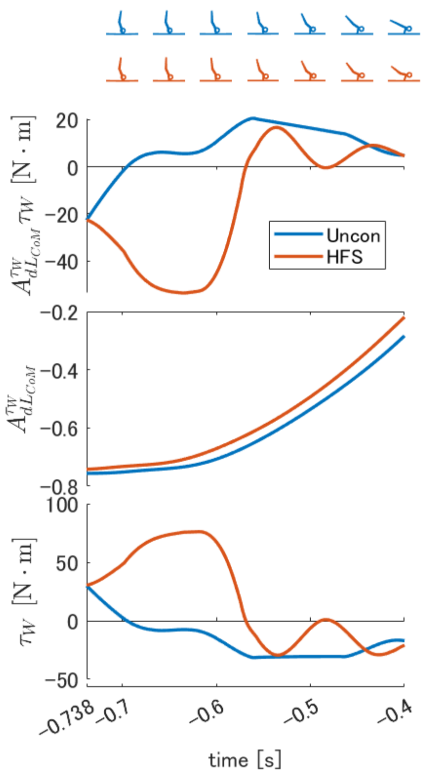

Figure 24: Breakdown of the wrist contribution to L_{CoM} ($= A^{\tau_W}_{dL_{CoM}} \tau_W$) into $A^{\tau_W}_{dL_{CoM}}$ and τ_W. From the top, $A^{\tau_W}_{dL_{CoM}} \tau_W$, $A^{\tau_W}_{dL_{CoM}}$, and τ_W are presented.

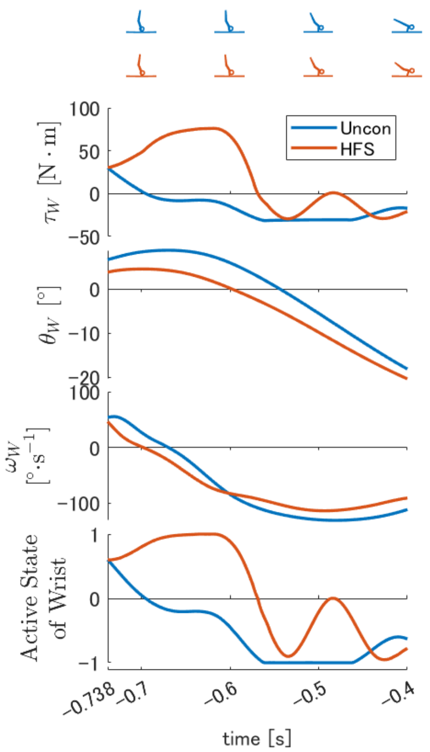

Figure 25: τ_W and the variables determining τ_W in [−0.738 s, −0.4 s]. From the top, τ_W, θ_W, ω_W, and the wrist active state are presented.

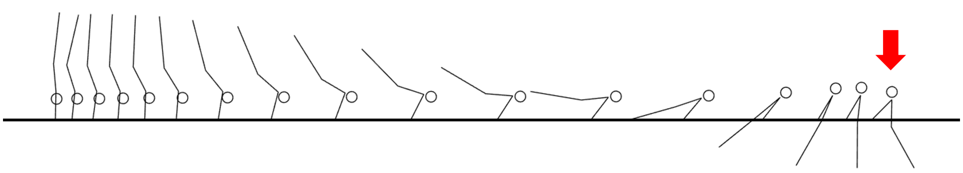

Figure 26: The simulated motion combining the active states in the two conditions. The active states are equal to those in the hip–flexion suppressed condition, except for the wrist active state after −0.738 s. The wrist active state after −0.738 s is equal to that in the unconstrained condition. θ_W becomes smaller than −45° at the moment indicated by the arrow, which satisfies the failure condition.

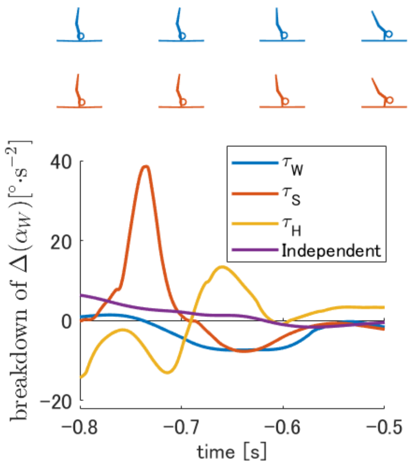

Figure 27: Difference in the contributions of τ_W, τ_S, τ_H, and the torque–independent term to α_W ($= \Delta(\alpha_W)$) between the two optimized conditions following Equation 18.

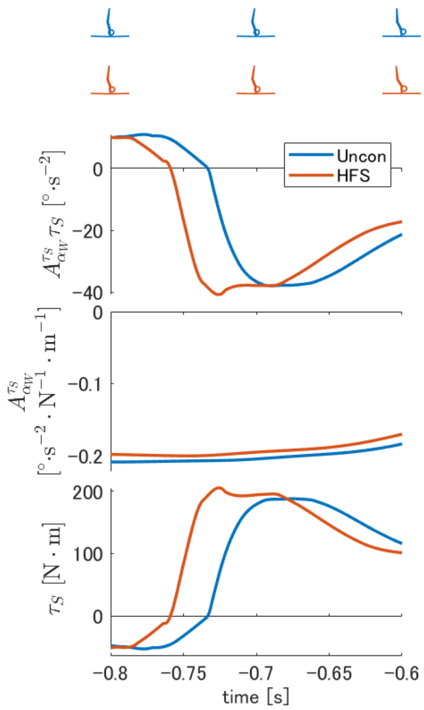

Figure 28: Breakdown of the shoulder contribution to $\alpha_W = (A^{\tau_S}_{\alpha_W}\tau_S)$ into $A^{\tau_S}_{\alpha_W}$ and τ_S. From the top, $(A^{\tau_S}_{\alpha_W}\tau_S)$, $A^{\tau_S}_{\alpha_W}$, and τ_S are presented.

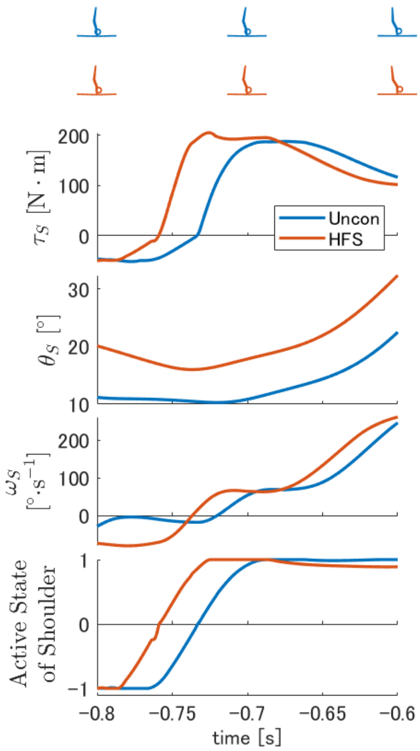

Figure 29: τ_S and the variables determining τ_S. From the top, τ_S, θ_S, ω_S, and the shoulder active state are presented.

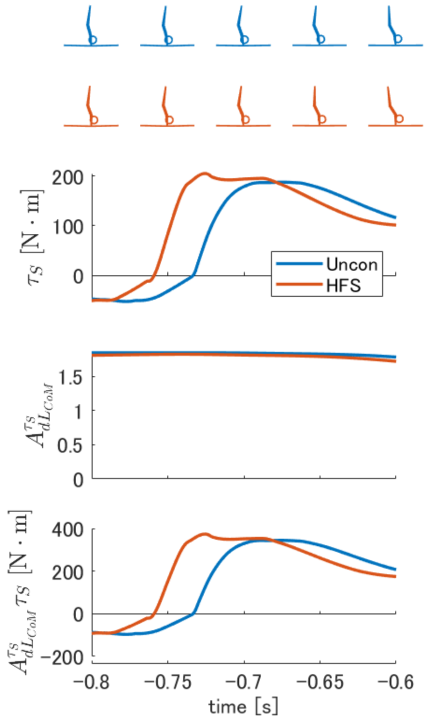

Figure 30: Breakdown of the τ_S contribution to L_{CoM} in $[-0.8\,\mathrm{s},\ -0.6\,\mathrm{s}]$. From the top, τ_S, $A^{\tau_S}_{dL_{CoM}}$, and $A^{\tau_S}_{dL_{CoM}}\tau_S$ are presented.

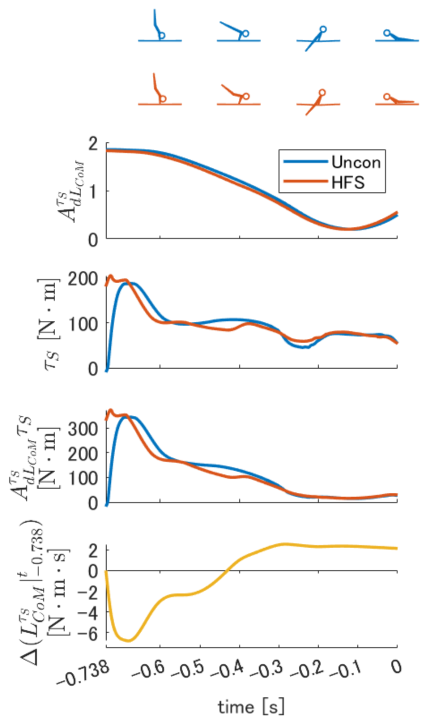

Figure 31: Difference in τ_S contribution to L_{CoM} and the relevant variables. From the top, $A^{\tau_S}_{dL_{CoM}}$, τ_S, $A^{\tau_S}_{dL_{CoM}}\tau_S$, and $\Delta(L^{\tau_S}_{CoM}|^{t}_{-0.738})$ after $-0.738\,\mathrm{s}$ are presented (Equation 15).

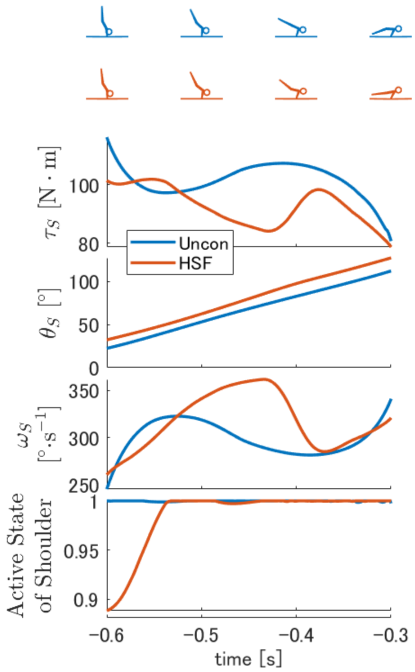

Figure 32: τ_S and the variables determining τ_S in $[-0.6\,\text{s}, -0.3\,\text{s}]$. From the top, τ_S, θ_S, ω_S, and the shoulder active state are presented.

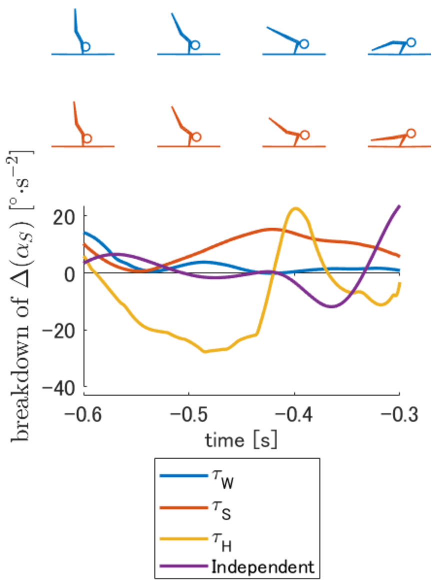

Figure 33: Difference in the contributions of τ_W, τ_S, τ_H, and the torque–independent terms to α_S $(= \Delta(\alpha_S))$ following Equation 19.

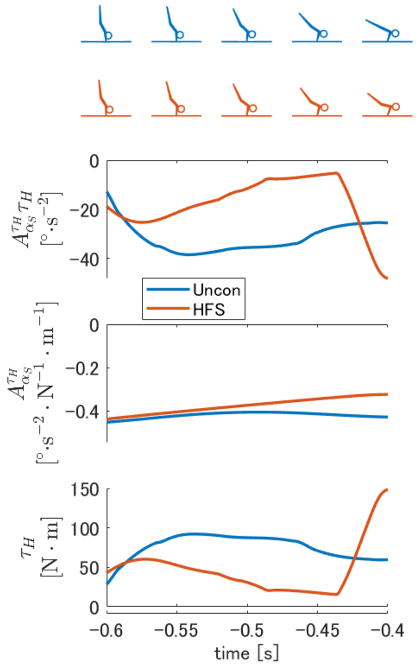

Figure 34: Breakdown of the hip contribution to α_S $(= A_{\alpha_S}^{\tau_H}\tau_H)$ into $A_{\alpha_S}^{\tau_H}$ and τ_H. From the top, $A_{\alpha_S}^{\tau_H}\tau_H$, $A_{\alpha_S}^{\tau_H}$, and τ_H are presented.

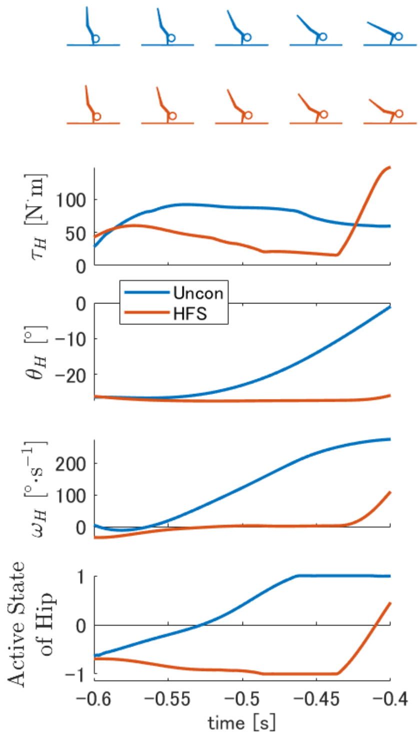

Figure 35: τ_H and the variables determining τ_H in $[-0.6\,\mathrm{s},\ -0.4\,\mathrm{s}]$. From the top, τ_S, θ_H, ω_H, and the hip active state are presented.